Environmental Science & Technology

pubs.acs.org/est

Article

Np(V) Retention at the Illite du Puy Surface

Bianca Schacherl, Claudia Joseph,* Aaron Beck, Polina Lavrova, Andreas Schnurr, Kathy Dardenne, Frank Geyer, Zara Cherkezova-Zheleva, Jörg Göttlicher, Horst Geckeis, and Tonya Vitova*

Cite This: *Environ. Sci. Technol.* 2023, 57, 11185−11194

Read Online

ACCESS | Metrics & More | Article Recommendations | Supporting Information

ABSTRACT: In this study, Np(V) retention on Illite du Puy (IdP) was investigated since it is essential for understanding the migration behavior of Np in argillaceous environments. The presence of structural Fe(III) and Fe(II) in IdP was confirmed by Fe K-edge X-ray absorption near-edge structure (XANES) and ^{57}Fe Mössbauer spectroscopy. In batch sorption experiments, a higher Np sorption affinity to IdP was found than to Wyoming smectite or iron-free synthetic montmorillonite. An increase of the relative Np(IV) ratio sorbed onto IdP with decreasing pH was observed by solvent extraction (up to (24 ± 2)% at pH 5, c_0(Np) = 10^{-6} mol/L). Furthermore, up to (33 ± 5)% Np(IV) could be detected in IdP diffusion samples at pH 5. Respective Np M_5-edge high-energy resolution (HR-) XANES spectra suggested the presence of Np(IV/V) mixtures and weakened axial bond covalency of the NpO_2^+ species sorbed onto IdP. Np L_3-edge extended X-ray absorption fine structure (EXAFS) analysis showed that significant fractions of Np were coordinated to Fe—O entities at pH 9. This highlights the potential role of Fe(II/III) clay edge sites as a strong Np(V) surface complex partner and points to the partial reduction of sorbed Np(V) to Np(IV) via structural Fe(II).

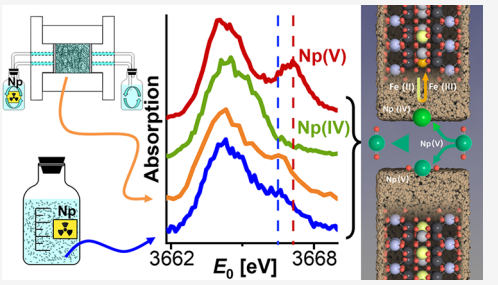

KEYWORDS: *neptunium, clay, high-energy resolution X-ray absorption near-edge structure (HR-XANES) spectroscopy, sorption, diffusion, solvent extraction*

INTRODUCTION

Many countries favor final disposal in deep geological formations as a long-term management strategy for high-level nuclear waste (HLW).[1−3] HLW contains long-lived radionuclides of high radiotoxicity[4] and redox sensitivity such as ^{237}Np. Pentavalent Np, Np(V), is stable under oxidizing to redox-neutral conditions. Np(V) can theoretically be present in the near-field of a repository through radiolysis or in disposal concepts where oxygen intrusion cannot be excluded.[5] The redox behavior of Np(V) might be also of interest in the context of contaminated land sites.[6] Np(V) forms a well-soluble[7] trans-dioxo ion (NpO_2^+) in aqueous solution. Tetravalent Np prevails under reducing conditions[8] and forms by about 5 orders of magnitude less soluble[9] hydroxo complexes.

Illite, a dioctahedral phyllosilicate, is a ubiquitous clay mineral in argillaceous rocks discussed as potential host rocks for nuclear waste repositories.[10−12] The structure of illite consists of two sheets of Si, which can be isomorphically substituted by Al^{3+} or Fe^{3+}, tetrahedrally (T) coordinated by oxygen and one sheet of Al, with potential isomorphic substitutions of Fe^{3+}, Fe^{2+}, or Mg^{2+}, octahedrally (O) coordinated by oxygen (TOT). The negative charge of the TOT layers, caused by these substitutions, is compensated by K^+ ions in the TOT interlayer space of illite.[13]

Np(V) sorption on illite (Na-Illite du Puy, IdP) was modeled by Bradbury and Baeyens[14] using data determined by Gorgeon[15] under aerobic conditions. The authors found moderate sorption for Np(V) with distribution coefficients of about log K_D = 1 to 2 L/kg (c_0(Np) = 10^{-6} mol/L) at neutral pH. However, the surface complexes were not investigated experimentally on a molecular scale. Marsac et al.[16] investigated the sorption of Np(V) on IdP under anaerobic conditions and found a higher log K_D. They concluded a partial reduction of Np(V) to Np(IV) on IdP surface at measured redox potentials (E_h referred to the standard hydrogen electrode), where only Np(V) species were expected to be present. The potential presence of structural Fe(II) as a redox partner was discussed as one possibility for the observed Np reduction. A thermodynamic sorption model based on measured E_h values was derived, resulting in thermodynamically favored Np(V) reduction in the presence of a sorbing mineral phase under given redox conditions.[16] In the literature, surface-mediated redox reactions of actinides are intensively

Received: December 11, 2022
Revised: May 28, 2023
Accepted: May 30, 2023
Published: July 17, 2023

investigated[17] and discussed.[18−20] On the one hand, proposed mechanisms involve the presence of structural or adsorbed Fe.[18] On the other hand, reduction of actinides on materials containing no Fe(II) as a reductant is reported.[19,20]

Due to the low hydraulic conductivity of clay rock ($<10^{-12}$ m/s),[21] diffusion is the predominant transport process for migrating Np when clay rock is used as geo-engineered barrier or host rock. Laboratory diffusion experiments focused on natural clay rocks, containing accessory Fe(II)-bearing minerals.[22−24] Spot-wise agglomerations of Np close to Fe(II)-bearing minerals were observed as well as a partial reduction to Np(IV). Alternatively, reducing conditions were induced by adding reducing agents such as $Na_2S_2O_4$ to the connected reservoir.[25] An increased level of Np sorption was found inferring the majority of Np to be present as Np(IV). Sorption and reduction during Np diffusion through pure clay minerals containing only structural Fe and no accessory Fe-bearing minerals were not investigated so far.

One powerful investigation method for studying the interaction of Np with clay is X-ray absorption spectroscopy (XAS). Np L_3-edge extended X-ray absorption fine structure (EXAFS) probes type, number, interatomic distances of atoms neighboring Np, and local structural disorder.[26] Recently, high-energy resolution X-ray absorption near-edge structure (HR-XANES) spectroscopy[27−31] at the Np M_5-edge was shown to be a valuable tool for oxidation state studies on Np loadings down to 1 ppm.[32−34] In addition, the Np M_5-edge HR-XANES spectra are very sensitive to changes of the Np bonding properties.[28,34]

This study combines different experimental approaches to study the role of Fe in the IdP structure on the Np retention in sorption and diffusion experiments. Fe K-edge XANES spectroscopy, ^{57}Fe Mössbauer spectroscopy, transmission electron microscopy (TEM), and fluorescence microscopy were applied for comprehensive characterization of Fe in IdP. Batch sorption data of Np on clay minerals with different Fe content were compared. Electronic structure, bonding properties, and local atomic environment of selected IdP samples were probed using Np M_5-edge HR-XANES and L_3-edge EXAFS spectroscopy. Complementary to the spectroscopic studies, solvent extraction[35] was carried out to determine fractions of Np(IV) and Np(V) sorbed on IdP as a function of pH and contact time (t_c). Similarly, Np was characterized in IdP segments as a function of diffusion depth.

MATERIALS AND METHODS

All experiments were performed under Ar atmosphere ($p(O_2)$ < 0.1 ppm; $p(CO_2)$ < 0.1 ppm) at room temperature (22 ± 1) °C, if not stated otherwise. Milli-Q water (18.2 MΩ·cm; Milli-Q Plus, Merck Millipore, Germany) was degassed by boiling and subsequently purged with Ar in three cycles before use.

Clays and Np Stock. In previous studies,[36,37] samples of IdP[38] were purified (procedure in SI 1) and characterized by X-ray fluorescence. The Fe_2O_3 content amounted to 6.94 wt.%.[37] This batch was referred to as IdP A. In the present study, IdP A was further characterized by ^{57}Fe Mössbauer spectroscopy, TEM−energy-dispersive X-ray spectroscopy (TEM-EDX), electron energy loss spectroscopy (EELS), and fluorescence microscopy (SI 1). Wyoming smectite (SWy) and illite samples referred to IdP B were treated with a slightly different conditioning procedure.[39] Iron-free synthetic montmorillonite (IfM) was obtained from the Laboratoire des Matériaux Minéraux (Mulhouse, France). It was synthesized in an acidic fluoride medium following Reinholdt et al.[40,41] The ^{237}Np(V) stock solution (c(Np(V)) = (6.0 ± 0.2) × 10^{-2} mol/L) was thoroughly characterized previously[42] and in equilibrium with its daughter nuclide ^{233}Pa.

Batch Sorption Experiments. Batch sorption experiments with ^{237}Np and IdP A or IdP B were performed at c_0(Np(V)) = 1 × 10^{-6} mol/L under anaerobic conditions (Ar, 1 ppm O_2 atmosphere) at pH 5, 7, and 9, under aerobic conditions at pH 5, and under anaerobic conditions at c_0(Np(V)) = 1 × 10^{-8} mol/L at pH 9 in quadruplicate. Batch sorption samples under anaerobic conditions with ^{237}Np and IdP B, SWy, or IfM were investigated at c_0(Np(V)) = 1 × 10^{-6} mol/L and c_0(Np(V)) = 1 × 10^{-8} mol/L in the pH range from 4.3 to 12. Precipitation of NpO_2(am) or Np(V) solid phases was not expected based on speciation calculations using PHREEQC[43] (version 3.4.0) and the thermodynamic model of Marsac et al.[16] under the chosen conditions. However, there is an uncertainty associated with E_h measurements in systems with low amounts of redox-active materials and suspensions. Therefore, the presence of Np solid phases was double-checked by EXAFS spectroscopy. All suspensions were preequilibrated in 0.1 mol/L NaCl to reach a solid-to-liquid ratio (S/L) of (2 ± 0.05) g/L (details in SI 2 and elsewhere[32]). Details on pH and E_h measurements are given in SI 3. Np was contacted with the clay suspensions from 7 to 1033 days. Subsequently, the samples were centrifuged (15,000 rpm = 12,500g, 80 min; LLG-uniCFUGE 5, Lab Logistics Group GmbH, Germany) and the amount of Np in the supernatant was determined by inductively coupled plasma−mass spectrometry (ICP−MS).

Diffusion Experiment. A ^{237}Np(V) through-diffusion experiment with cylindrically compacted IdP A (sample length: 11.5 mm, diameter: 25.6 mm, dry density: 1600 kg/m^3) was conducted under aerobic conditions according to the procedure described in Van Loon et al.[44] The clay-confining diffusion cell was connected on each end plate to a reservoir, respectively, filled with 0.1 mol/L NaCl at pH 5. The clay was conditioned for 6 months. Subsequently, one reservoir was replaced by the "source" reservoir containing the tracer (V = 100 mL, c_0(Np(V)) = 1.4 × 10^{-5} mol/L ≡ 90 Bq/g, I = 0.1 mol/L NaCl, pH 5). The other reservoir (V = 20 mL) was referred to as the "receiving" reservoir. It was regularly replaced by receiving reservoirs with fresh tracer-free electrolyte solution. The diffusion experiment was terminated after 1050 days. The diffusion sample was introduced into an Ar box and separated in cylinder length steps of about 100 μm in 103 segments (details in SI 4 and elsewhere[45]).

Solvent Extraction and Acid Digestion. Batch sorption samples in quadruplicate and every 5th segment of the diffusion sample were analyzed by solvent extraction (details in SI 5) according to the procedure of Bertrand and Choppin.[35] With this method, the fractions of sorbed Np(V) (dissolved in the aqueous phase) and sorbed Np(IV) (dissolved in the extractant) on IdP A and B were determined. The clay, the aqueous phase, and the extractant, containing xylene and 2-thenoyltrifluoroacetone, were vigorously shaken for 10 min and then carefully separated by centrifugation (15,000 rpm (= 12,500g), 80 min). In the case of the batch sorption samples, the extractant was back extracted with 8 mol/L HNO_3 (see flow chart in SI 5). Both, the aqueous phase and the HNO_3 extract of the organic phase were analyzed for ^{237}Np content by ICP−MS. After solvent extraction, the clay residue of one

https://doi.org/10.1021/acs.est.2c09356
Environ. Sci. Technol. 2023, 57, 11185−11194

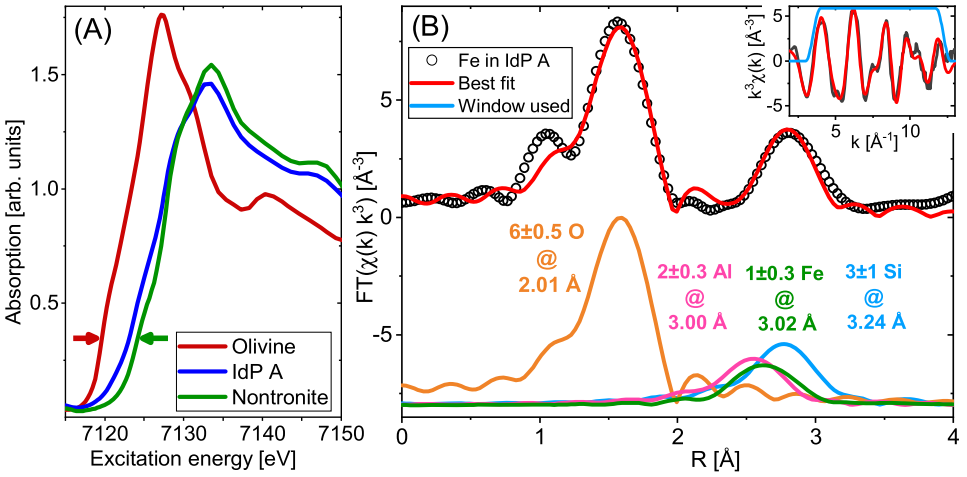

Figure 1. (A) Fe K-edge XANES spectra of olivine (red), IdP A (blue), and nontronite (green). The first inflection points of nontronite and olivine are marked with an arrow. (B) EXAFS spectrum in *R*-space of Fe in IdP A (black circles) and the best fit (red line). The contributions of each path are shown vertically shifted. The k^3-weighted $\chi(k)$ (black line), the used window (blue line), and the best fit (red line) are in the embedded figure (top right).

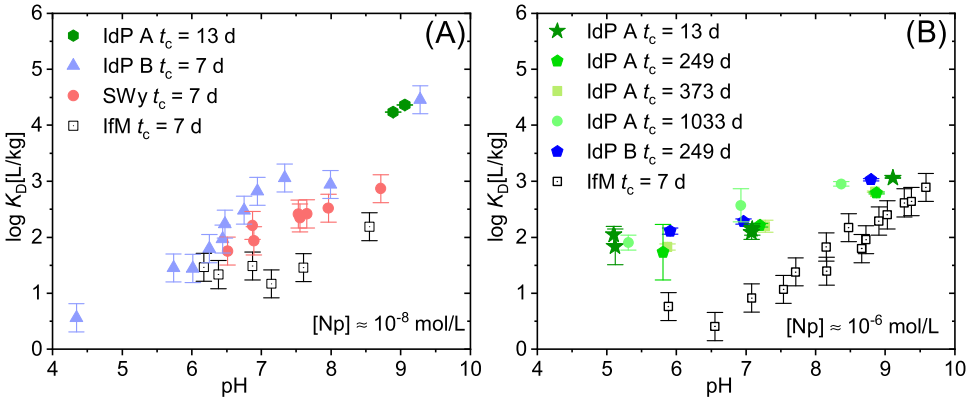

Figure 2. Distribution coefficients (log K_D) of Np(V) on clay minerals (A) in dependence on pH at c_0(Np(V)) = 1 × 10^{-8} mol/L; (B) log K_D of Np(V) in dependence on pH and contact time (t_c) at c_0(Np(V)) = 1 × 10^{-6} mol/L; Illite du Puy (IdP A—green signs, IdP B—blue signs),[51] Wyoming smectite (SWy—red circles),[52] Fe-free montmorillonite (IfM—empty black squares).[40] The error bars refer to ±0.25 log K_D units on the single sorption experiments and to the 95% confidence interval of the quadruplicate sorption experiments.

single extraction sample of each batch sorption experiment was digested in acid (HNO_3/HCl/HF) to determine the non-desorbable fraction of Np. To determine the amount of total Np in the diffusion segments, 15 mg (± 0.5 mg) of each segment was extracted for 5 days with 4 mol/L HNO_3 and analyzed with liquid scintillation counting (LSC, SI 6).

Samples Studied with X-ray Absorption Spectroscopy. Np present in only one oxidation state, i.e., Np(IV) or Np(V) (c(Np) = 0.02 mol/L), in aqueous solutions were used as reference samples. To obtain Np(IV), ion exchange resin purified and isotopically pure 0.02 mol/L ^{237}Np(V) in 1.5 mol/L HCl was electrochemically reduced using a Pt mesh type working electrode, a Pt rod type counter electrode, a Ag/AgCl reference electrode in 3 mol/L KCl at +0.30 V vs Ag/AgCl, and a potentiostat (scanning potentiostat model 362, Princeton Applied Research).

Three types of solid XAS samples were prepared: (1) pure IdP A samples, (2) IdP A from Np batch sorption experiments after centrifugation, and (3) about 2 mg of ground IdP A segments of the diffusion experiment at varying diffusion depths. All samples were placed in sample holders specifically designed for these experiments and were encapsulated with two barriers of Kapton (8 μm) under inert gas atmosphere (SI 7).

The samples were studied with Np M_5-edge HR-XANES and Np L_3-edge EXAFS spectroscopy at the ACT part of the CAT-ACT beamline for catalysis and actinide science at the KIT Light Source (KLS), Karlsruhe, Germany.[46] Further details on the beamline and experimental conditions can be found in SI 8. Beam-induced changes in Np oxidation state were excluded by extensive testing with various methods.[32] The oxidation state of Fe in IdP A was examined via Fe K-edge XANES spectroscopy at the Synchrotron Laboratory for Environmental Studies (SUL-X) beamline[47] also at KLS (cf. SI 9). For analysis of the XAS spectra, the programs Origin, ATHENA, and ARTEMIS[48] were used (SI 10).

RESULTS AND DISCUSSION

Characterization of IdP A. A detailed discussion of the characterization results can be found in SI 11. Briefly, the comparison of the Fe K-edge XANES spectra inflection points of nontronite (Fe(III)-rich smectite) and olivine (Fe(II) neosilicate) with IdP A (Figure 1A) showed that Fe is predominantly present as Fe(III) with a minor fraction of

https://doi.org/10.1021/acs.est.2c09356
Environ. Sci. Technol. 2023, 57, 11185−11194

Fe(II) in IdP A. Fe K-edge EXAFS spectroscopy (Figure 1B and Table SI 2) allocated Fe as predominantly present in the octahedral sheets of IdP A. Both, EXAFS and TEM−energy-dispersive X-ray spectroscopy (EDX) (Figures 1B and SI 6) identified a homogeneous distribution of Fe across the clay sample and the absence of Fe oxide nanoparticles. Furthermore, crystallites of a Ca-phase were found in IdP A by TEM and EELS. Bradbury and Baeyens[39] removed the Ca-silicate phase in their illite purification procedure, applied in the present study to purify IdP B. To examine if this phase has an effect on Np sorption, illite batches with (IdP A) and without (IdP B) this phase were investigated in Np batch sorption experiments in this study. ^{57}Fe Mössbauer spectroscopy (Figure SI 8 and Table SI 3) found approximately (34.0 ± 0.5) at.% Fe(III) in octahedral sheets, (58.0 ± 0.5) at.% Fe(III) in tetrahedral sheets, (6.0 ± 0.5) at.% Fe(II) in octahedral sheets, and (2.0 ± 0.5) at.% Fe(II) in tetrahedral sheets of IdP A. The exact quantification of the actual redox-active Fe is not trivial;[49,50] however, the fact that Fe(II) exists in IdP in a low percentage is of relevance for the present study. Fluorescence microscopy with live-death staining (Figure SI 9) confirmed no living or dead organic matter in the clay. The results of all of the various analysis methods combined excluded the presence of microorganisms and Fe oxide nanoparticles in the IdP A batch and hence, confirmed that the only redox-couple present in IdP A was structural Fe(II)/Fe(III). The presence of structural Fe(II) in the IdP despite purification under aerobic conditions is surprising and needs further investigation.

Sorption and Solvent Extraction Results. *Sorption of Np on IdP A, IdP B, SWy, and IfM.* Np(V) sorption was studied for three different clay minerals (Figure 2 and Table SI 4). Although the structural Fe in IdP A was thoroughly characterized and the presence of Fe oxide nanoparticles and microorganisms excluded, in the case of IdP B, SWy, and IfM, no such detailed characterization was performed. However, the materials were characterized previously.[39,53−55] Consequently, the presence of Fe oxide nanoparticles in the clay suspensions could be excluded for all clays studied. In comparison to SWy, IdP A, and IdP B, Np(V) exhibited the lowest log K_D onto IfM (Figure 2A,B). A slightly increased log K_D was noticeable for Np(V) sorbed on SWy. The highest log K_D was found for Np(V) onto IdP A and IdP B. The clay minerals contained about 3.7 wt.% Fe_2O_3 (SWy) and 6.94 wt.% Fe_2O_3 (IdP A/B), respectively.

In the literature, differing sorption affinities are sometimes related to differing surface areas of the studied sorbent.[56] However, in this study, the N_2-BET surface areas of IdP B (97 m^2/g),[39] SWy (35 m^2/g),[55] and IfM (123 m^2/g)[54] could not account for the differences in sorption. The total amount of sorbed Np increased in all cases with increasing pH due to increasing clay edge-site deprotonation.[14,54,57] The contact time beyond 13 days did not seem to influence the total amount of sorbed Np on IdP (Figure 2B). This is in accordance with the findings of Marsac et al.[16] The comparison of the sorption data of illite treated with different purification procedures, namely, IdP A and IdP B (Figure 2), did also not show a significant difference in the overall Np sorption. Since there is no difference between IdP A and B, the Ca-phase crystallites detected in IdP A by TEM (Figures SI 6 and 7) probably did not play a major role in the sorption of Np. K_D values for both initial Np concentrations (c_0(Np(V)) = 1×10^{-8} mol/L and 1×10^{-6} mol/L) are congruent to those found by Marsac et al.[16] Note, the lower log(K_D) values for the IdP samples at higher Np(V) concentrations cannot be attributed to a strong/weak site complexation effect because the Np loading at 1×10^{-6} mol/L Np was still significantly below the available amount of strong sites at pH 7 and 9 (2×10^{-6} mol/g × 2 g/L = 4×10^{-6} mol/L).[58] Consequently, the strong sites should not be saturated with Np in this pH range. Np(V) sorption onto IdP under aerobic conditions and published by Bradbury and Baeyens[14] showed similarly low sorption as obtained in this study for IfM. Marsac et al.[16] explained the differences in Np(V) sorption on IdP under anaerobic conditions and those of Bradbury and Baeyens[14] under aerobic conditions by a surface-induced reduction of Np(V) to Np(IV). Since Np(IV) exhibits stronger sorption onto surfaces than Np(V), this indicates that more Np(IV) is formed under anaerobic conditions. A higher Np(IV) fraction at lower total Np loading also explains the increased log K_D at a low initial Np concentration.

Solvent Extraction of Np Sorbed on IdP A. In order to verify the assumption of Np(V) reduction at IdP surfaces, solvent extraction experiments were carried out with Np batch sorption samples of contact times up to t_c = 1033 days (Table SI 5). The amount of Np left on the clay after solvent extraction was determined by total acid digestion of some samples since mass balance calculations revealed that a certain fraction of Np did not desorb. Surface-sorbed Np(V) should be very easily desorbable. The strong binding of Np to clay even under acidic conditions is, thus, explained by the reduction of Np(V) to strongly binding Np(IV) species. In Table SI 5, this fraction is assigned as "Np(IV) clay digestion" and added to the Np(IV) fraction determined by solvent extraction (before digestion "Np(IV) desorbed"; after digestion "total Np(IV) on illite" Table SI 5). Even then, mass balance calculations revealed that a part of Np (≈ 6 to 18% of the initially added Np in the majority of samples) could not be recovered. Consequently, the Np(IV) fraction in Table SI 5 can be considered as lower limit. The nonretrievable fraction could be Np lost by wall sorption during the various processing steps.

The fraction of total Np(IV) on illite detectable by solvent extraction and clay digestion increased with decreasing pH. The fraction of total Np(IV) was very small at pH 9 − between 2 and 10%. At these low amounts, the uncertainties become significant. At pH 7, the relative amount of Np(IV) ranged from 6 to 15% (Table SI 5). At pH 5, the corresponding digestion and solvent extraction yielded a Np(IV) fraction of 11 to 24%. In order to rationalize this observation, one may have another look to Figure 2B. Sorption data revealed that at near-neutral pH, the extent of Np(V) sorption onto IdP is significantly increased relative to the sorption on IfM. Assuming surface-mediated reduction taking place as proposed in the literature, this is the consequence of the much stronger sorption of Np(IV) than of Np(V) notably at low pH. The difference in distribution coefficient, K_D, values clearly decreases at high pH, indicating that the thermodynamic driving force for Np(V) reduction to Np(IV) is higher at low pH than at high pH. The experimentally observed increase of Np(IV) with decreasing pH is compatible with the variation in sorption and thermodynamic considerations.

In a further test, the Np sorption onto IdP A at aerobic and anaerobic conditions at pH 5 was compared. NpO_2^+(aq) dominated the solution speciation in both systems. IdP A contained, also under aerobic conditions, structural Fe(II).

https://doi.org/10.1021/acs.est.2c09356
Environ. Sci. Technol. 2023, 57, 11185−11194

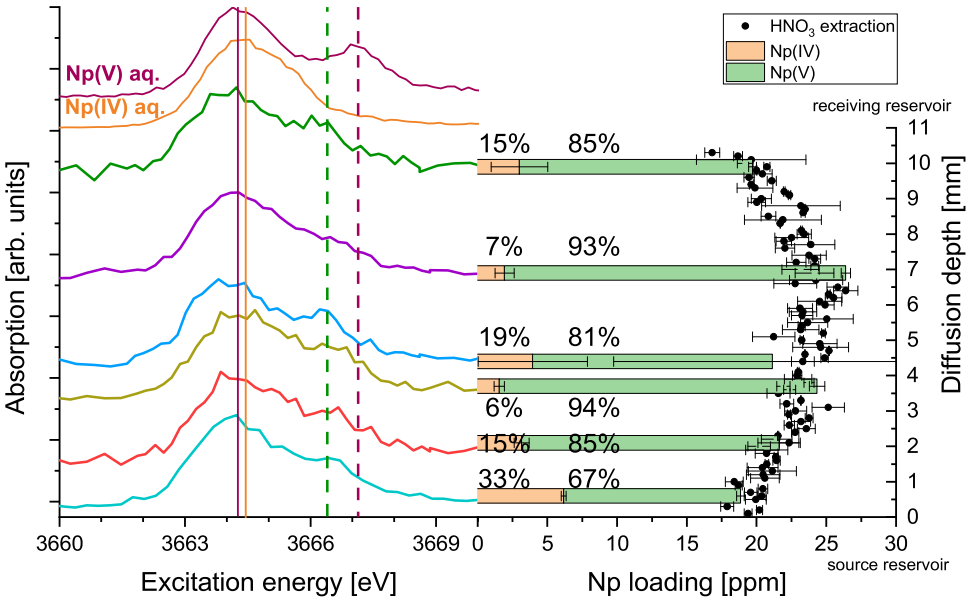

Figure 3. (Left) Vertically shifted Np M_5-edge HR-XANES spectra of selected diffusion segments and aqueous Np(IV) and Np(V) reference solutions. (Right) Amounts of Np(IV) in orange and Np(V) in green found by solvent extraction in the desorbable fraction of Np from the IdP A segments between 0.6 and 9.6 mm diffusion depth. Black dots indicate the amount of Np desorbed by oxidative acid extraction.

The average distribution coefficient after t_c = 11 days amounted to $\log K_D$ = (1.27 ± 0.19) L/kg under aerobic conditions and $\log K_D$ = (1.9 ± 0.1) L/kg under anaerobic conditions. In the aerobic samples, the redox potential, E_h, was controlled by dissolved oxygen, which caused a decreased amount of sorbed Np(IV) resulting in a lower amount of total sorbed Np. The E_h values in the anaerobic sorption sample were significantly lower compared to the aerobic experiment and controlled by the Fe(II)/Fe(III) couple of IdP A. However, reliable E_h measurements in systems with low concentrations of redox pairs are difficult.

While the general trend of experimental redox speciation data is compatible with the assumed surface-mediated reduction concept, the presented results are in some disagreement with respect to the quantity of reduced Np compared to the data reported by Marsac et al.[16] They found a sorbed Np to Np(IV) reduction of (41 ± 10) % for the extraction of one sample at pH 7, which is higher than the 6 to 15% measured in the present study. However, Marsac et al.[16] proposed for their L_3-edge XANES analysis samples only 14% Np(IV) contribution at pH 7.4 and 5% Np(IV) at pH 9.6.[16]

The origin of the analytical deviations for Np(IV) is presently unclear. Differences in the outcome of solvent extraction experiments might be due to different experimental boundary conditions (extracting agents, contact times) or reoxidation during the extraction. In the case of ^{237}Np quantification by LSC as described in Marsac et al.,[16] matrix effects may have interfered the α/ß-discrimination, resulting in incomplete separation of the high energetic ß$^-$-radiation of ^{233}Pa from the α-radiation of ^{237}Np. Both artifact types can result in under- and overestimation of Np(IV) fractions, respectively. For this reason, ICP−MS was used as the ^{237}Np detection method in the batch sorption experiments in the present study. In addition, special care was taken to purify the solvents from oxygen impurities before use in the experiments.

Solvent Extraction of Np in Diffusion Samples. A diffusion experiment with compacted IdP A and Np(V) was conducted at pH 5 for 1050 days to study the clay-induced Np(V) reduction at a higher S/L ratio and under dynamic conditions.[44] The Np diffusion profile was determined by acid and solvent extraction for six segments representing diffusion depths ranging from 0.6 to 9.6 mm. Np(IV) and Np(V) contents above the detection limit (2 ppm) were detected in every clay segment extracted. The Np(IV) content ranged from (7 ± 2)% to (33 ± 5)% of extracted Np with strong scattering throughout the diffusion sample (Figure 3). Detailed results of this diffusion experiment are reported in Beck et al.[45] It is however interesting to note that modeling results of the in- and out-diffusion data during the first 230 days (referred to as Np-2 in Beck et al.[45]) resulted in a relatively high $\log K_D$ = (1.78 ± 0.04) L/kg which resembles the K_d value measured in the anaerobic sorption samples (Table SI 4). Such a high K_d value is incompatible with the sorption of Np(V) to IdP (see discussion above) and can be explained by a much lower oxygen abundance in the pore system compared to the aerobic conditions in the reservoirs, which results in the partial reduction of the Np(V) on the clay.

The range of 7−33% Np(IV) in the clay determined in this study, is lower than 63% Np(IV) found onto bentonite by Xia et al.[25] In contrast to the here analyzed experiment with an E_h (source reservoir solution) of about 350−500 mV, Xia et al.[25] added $Na_2S_2O_4$ to the source reservoir solution which lead to an E_h of about −200 to −400 mV. E_h values in the pore volume are difficult to measure so that further analysis of the diffusion profile by reactive transport modeling could help to clarify the distinct contributions of Np sorption and reduction processes on diffusive transport. Reich et al.[23] found (80 ± 5)% Np(IV) at 450 μm and (26 ± 5)% at 525 μm diffusion distance by Np L_3-edge XANES spectroscopy for the Np diffusion through Opalinus Clay. They attributed it to the presence of accessory Fe(II)-mineral phases such as pyrite which were detected but not quantified as a function of depth. Invasive speciation techniques such as extractions, where chemical conditions are significantly varied during the analysis, can be subject to systematic errors to some extent. For this reason, the segments were also analyzed spectroscopically.

https://doi.org/10.1021/acs.est.2c09356
Environ. Sci. Technol. 2023, 57, 11185−11194

Spectroscopic Findings. *Np M_5-edge HR-XANES Spectroscopy of Np Sorbed on IdP A.* The spectra of Np(V) and Np(IV) aqueous reference solutions (c(Np) = 20 mmol/L) and of three batch sorption samples (pH 5 and 9) are depicted in Figure 4. The different features are described in detail in

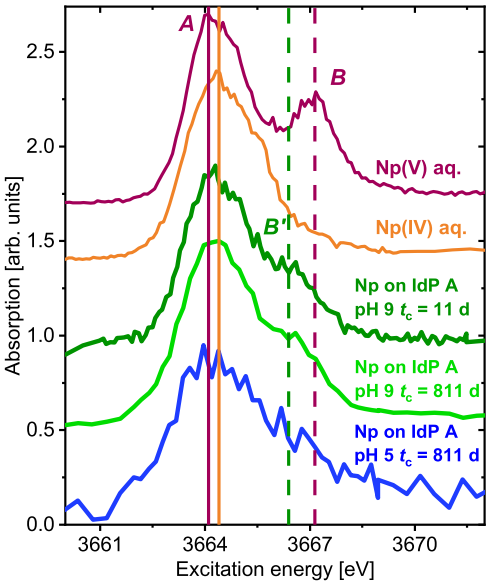

Figure 4. Np M_5-edge HR-XANES spectra of Np(V) and Np(IV) in aqueous solution and Np sorbed on IdP A at pH 9 after 11 and 811 days of contact time as well as Np sorbed on IdP A at pH 5 after 811 days of contact time. For a better comparison, the spectra were vertically shifted.

Schacherl et al.[32] Briefly, the spectrum of $Np(V)_{aq}$ shows a strong peak at 3664.1 eV (A) and a distinct shoulder at 3667.14 eV (B). Feature B can be correlated with the 3d transition to the unoccupied σ^* orbital of the axial Np—O bond.[28,32,34] The spectrum of $Np(IV)_{aq}$ exhibits a relatively broad white line (WL) with its maximum (A) trending to slightly higher excitation energies compared to A of $Np(V)_{aq}$ but descends quickly hereafter. The spectrum of Np sorbed on IdP A at pH 9 shows a feature B' shifted to lower energies compared to feature B in the spectrum of $Np(V)_{aq}$, pointing to a decreased bond covalency of Np—O_{ax}. The energy position of the first intense peak A is similar for $Np(V)_{aq}$ and Np sorbed onto IdP A. This observation indicates a similar electron density on the central Np atom despite decreased Np—O_{ax} bond covalency. This suggests stronger covalent interaction between the Np(V) sorbed and O_{eq} of the clay binding site compared to $Np(V)_{aq}$. Similar empirical observations have been made for U(V) complexes (compounds 2 and 7).[59] Lower U—O_{ax} bond covalency was found for 2, but the electronic density on U remained similar as a result of differences in the U-equatorial ligand interaction. Additionally, the intensity of the shoulder B' is lower in comparison to shoulder B, indicating that a fraction of Np(IV) might also be present.

The sample at pH 9 was studied after t_c = 11 days and after t_c = 811 days. A clear improvement in signal-to-noise ratio despite shorter acquisition time is visible (Figure 4), which was achieved due to improvements in the experimental setup at the beamline.[32,33] Nevertheless, the spectral features remained the same, an indication that no significant changes in the Np(IV)/Np(V) ratio on the IdP A at pH 9 occurred even after longer contact times.

The HR-XANES spectrum of the pH 5 batch sorption sample after 811 days is also displayed in Figure 4. A high noise level is preventing a detailed examination. However, the trend of a broader WL feature A and a lower intensity of feature B' than in the pH 9 sample seems to progress, thus resembling slightly more the $Np(IV)_{aq}$ spectrum. This hints at a substantial Np(IV) amount in the batch sorption sample at pH 5. The fraction of 11 to 24% Np(IV) found by solvent extraction seems to be in agreement with this finding. The lack of appropriate Np reference compounds hindered the quantification of the Np(IV)/(V) ratio from the HR-XANES spectral data. An appropriate Np reference system would consist of an experiment, where redox conditions are controlled in order to assure that clay adsorbed Np is either pentavalent or tetravalent.

Batch sorption and spectroscopy studies appear to support the interpretation of Marsac et al.[16] of surface-mediated reduction. Note, the amounts of Np(IV) found here were

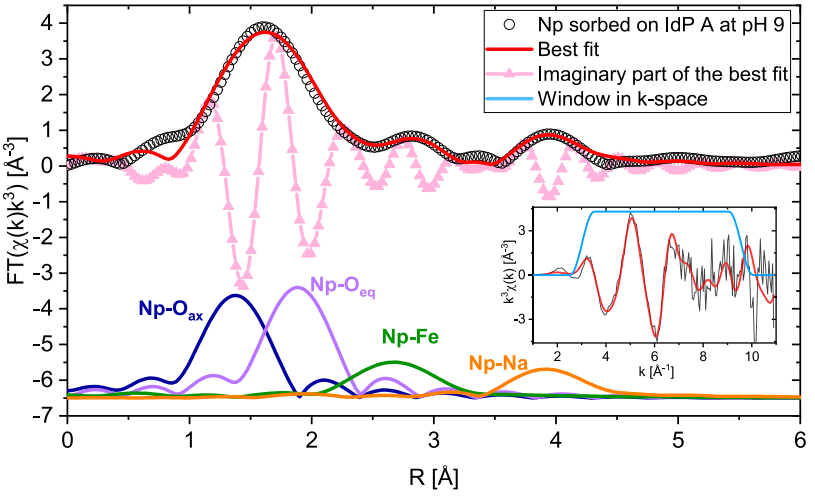

Figure 5. Fourier-transformed EXAFS spectrum in R-space of Np sorbed on IdP A at pH 9 (black circles), the imaginary part (rose triangles), and the best fit (red line). The contributions of each path are shown vertically shifted. Embedded is the k^3-weighted $\chi(k)$ (black line), the used window (blue line), and the best fit (red line).

https://doi.org/10.1021/acs.est.2c09356
Environ. Sci. Technol. 2023, 57, 11185−11194

lower than postulated by Marsac et al.[16] The respective mechanistic discussion listed structural Fe(II) as a possible reductant inducing a relatively low redox potential. Furthermore, Ma et al.[60] listed Fe(II)-containing minerals including clay minerals with structural Fe(II) as the main electron donor for the retention mechanisms of redox-sensitive radionuclides.

Speciation of Np Diffused through Illite. The same diffusion segments as investigated by leaching and solvent extraction with Np contents down to (18 ± 1) ppm were selected for further spectroscopic analysis. For the first time, these kinds of samples were studied by Np M_5-edge HR-XANES spectroscopy (Figure 3). As for the batch sorption samples, all spectra showed feature *B′* with variable intensity and a broader feature *A*, which implied the presence of Np(V) and Np(IV) in all segments. This indicated that a partial reduction of Np(V) to Np(IV) took place by IdP A during the diffusion process. The energy difference between features *A* and *B′* was similar to the energy shift detected in the batch sorption samples (Figure 4), suggesting a similar Np(V) species on the IdP A surface. In conclusion, also in this case, a reduction reaction controlled by structural Fe(II) in IdP A seemed to have occurred. This supports the findings of the extraction studies: While aerobic conditions prevail in the reservoirs, structural Fe(II) in the clay plug is capable to buffer the E_h in the pore space and to establish a more reducing environment.

Np L_3-Edge EXAFS Spectroscopy of Np Sorbed on IdP A. Np(V) reduction by structural Fe(II) requires close interaction of Np(V) with Fe in order to allow for electron transition. To examine the Np coordination environment, the EXAFS spectrum (Figure 5) of an IdP A batch sorption sample at pH 9 was analyzed. The analysis confirmed the presence of solely sorbed mononuclear Np species, since the spectrum did not reveal any Np—O—Np coordination characteristic for NpO_2 precipitates, in contrast to studies using higher initial Np concentrations such as Kumar et al.[61] The EXAFS analysis (Table SI 6) yielded two O atoms at a relatively short Np—O distance of (1.86 ± 0.01) Å, which were attributed to the axial O atoms of the NpO_2^+ ion (O_{ax}). The O_{ax} distances reported in the literature for $Np(V)_{aq}$ range from (1.80 ± 0.02) Å[62] to (1.84 ± 0.01) Å.[63] For sorbed Np(V) species, slightly longer Np—O_{ax} distances of (1.840 ± 0.006) Å on gibbsite at pH 7.5,[64] (1.86 ± 0.002) Å on corundum at pH 9,[65] or (1.887 ± 0.006) Å for Np(V) carbonate on hematite at pH 8.81[66] were reported. The Np—O_{ax} distance found for Np on IdP A is comparable to literature data reported for surface-sorbed Np(V) species. In addition, a Np—O distance of (2.41 ± 0.01) Å with a coordination number of N = 4.0 ± 0.3 was detected for Np on IdP A at pH 9. This could be assigned to water molecules and illite hydroxyl groups in the equatorial plane of NpO_2^+ (O_{eq}). This distance is not only shorter than the Np—O_{eq} in $Np(V)_{aq}$ (2.484 to 2.49 Å),[62,63] but also shorter than found for Np(V) sorbed onto corundum[65,67] and gibbsite[64] (2.45 to 2.50 Å). This hints at a stronger chemical bonding in the equatorial plane for Np on IdP A. This might also be the consequence of a partial reduction of Np(V) to Np(IV), since Np—O distances for sorbed Np(IV) were found to lie for the first shell between 2.24 and 2.27 Å and for the second shell between 2.41 and 2.44 Å.[68]

A Np—Fe coordination shell was found at (3.05 ± 0.02) Å suggesting that Np surface species were in close proximity to Fe (N(Fe) = 1.0 ± 0.3) in IdP A. Al and Si, potentially present in the second coordination sphere of Np on the IdP A surface, were tested during the modeling of the EXAFS spectrum, too. However, a reasonably good fit (goodness of fit = 0.013 χ^2) was only obtained considering Fe. An additional contribution of Al to the second peak was not excluded; however, this mixed model would be oversampling the data since the fit did not significantly improve with the addition of this path. In addition, a Np—Na coordination was postulated at a distance of (4.34 ± 0.03) Å. This scattering path is reasonable since Na ions are present in the electrolyte solution and are coordinated at the basal surfaces and at the clay edges around the surface-sorbed Np for charge compensation. Other potentially present cations, such as Np, Al, Si, Mg, or K, were not appropriate to model this feature. The absence of a Np—Np scattering path verified that Np was present as a solely sorbed species on the clay surface and no Np solid phases had formed. The results suggest that Np(V) sorbed onto IdP A is coordinated to the partially deprotonated hydroxyl groups surrounding the Fe atoms on the clay surface. The finding that Np is coordinated to Fe, in combination with the results of solvent extraction and HR-XANES spectroscopy, points to Fe—O entities as a strong complexation partner. The coordination of Cm(III) to Fe—OH entities of IdP was also discussed by Rabung et al.[69] in a time-resolved laser-induced fluorescence spectroscopy study. Due to a strong decrease in fluorescence intensity as a result of static quenching, they concluded that a part of surface-complexed Cm(III) must be directly coordinated to Fe—OH groups. The presence of surficial Fe—OH ligands at clay edges is likely due to the Fe/Al ratio of 0.3 in IdP.

■ ENVIRONMENTAL IMPLICATIONS

The exact mechanism of redox-sensitive radionuclide interaction with Fe(II)-containing clays is still controversially discussed. Literature studies proposed that electrons in Fe-containing clay minerals can be transferred either via Np interaction with edge-site Fe(II)—O—Fe(III) groups,[18] octahedral Al/Fe(II)—OH[60] sites, or even with the basal planes.[70] In the present study, Fe(II) was detected in IdP A by ^{57}Fe Mössbauer and K-edge XANES spectroscopy even though the clay was previously treated and purified under aerobic conditions. Moreover, it was shown that structural Fe in IdP A was associated with Np(IV)/Np(V). It was hypothesized that Fe(II/III) clay edge sites represent a strong complexation partner and a possible source of reduction since Np(IV) was found in sorption as well as diffusion samples, particularly, at lower pH values (pH 5). Advanced X-ray absorption spectra suggested that strong equatorial binding to Fe(II)/Fe(III)—OH entities was likely responsible for the reduction of the axial bond covalency of the Np(V). Since clay minerals containing Fe(II/III) are abundant in environmental samples profound understanding of redox-sensitive element interaction with respective minerals requires more studies using sensitive spectroscopic methods. This study advances the understanding of the mechanism behind strong Np retention in some clay systems relevant in the context of contaminated land sites and nuclear waste disposal.

■ ASSOCIATED CONTENT

Supporting Information

The Supporting Information is available free of charge at https://pubs.acs.org/doi/10.1021/acs.est.2c09356.

Experimental details on materials, methods, as well as detailed sample and EXAFS data tables (PDF)

https://doi.org/10.1021/acs.est.2c09356
Environ. Sci. Technol. 2023, 57, 11185−11194

AUTHOR INFORMATION

Corresponding Authors

Claudia Joseph − *Karlsruhe Institute of Technology (KIT), Institute for Nuclear Waste Disposal (INE), D-76021 Karlsruhe, Germany;* orcid.org/0000-0003-3975-8647; Email: claudia.joseph@gmx.net

Tonya Vitova − *Karlsruhe Institute of Technology (KIT), Institute for Nuclear Waste Disposal (INE), D-76021 Karlsruhe, Germany;* orcid.org/0000-0002-3117-7701; Email: tonya.vitova@kit.edu

Authors

Bianca Schacherl − *Karlsruhe Institute of Technology (KIT), Institute for Nuclear Waste Disposal (INE), D-76021 Karlsruhe, Germany;* orcid.org/0000-0003-4542-0108

Aaron Beck − *Karlsruhe Institute of Technology (KIT), Institute for Nuclear Waste Disposal (INE), D-76021 Karlsruhe, Germany*

Polina Lavrova − *Karlsruhe Institute of Technology (KIT), Institute for Nuclear Waste Disposal (INE), D-76021 Karlsruhe, Germany*

Andreas Schnurr − *Karlsruhe Institute of Technology (KIT), Institute for Nuclear Waste Disposal (INE), D-76021 Karlsruhe, Germany*

Kathy Dardenne − *Karlsruhe Institute of Technology (KIT), Institute for Nuclear Waste Disposal (INE), D-76021 Karlsruhe, Germany*

Frank Geyer − *Karlsruhe Institute of Technology (KIT), Institute for Nuclear Waste Disposal (INE), D-76021 Karlsruhe, Germany*

Zara Cherkezova-Zheleva − *Institute of Catalysis, Bulgarian Academy of Sciences, 1113 Sofia, Bulgaria;* orcid.org/0000-0002-9287-3217

Jörg Göttlicher − *Karlsruhe Institute of Technology (KIT), Institute for Photon Science and Synchrotron Radiation (IPS), D-76021 Karlsruhe, Germany*

Horst Geckeis − *Karlsruhe Institute of Technology (KIT), Institute for Nuclear Waste Disposal (INE), D-76021 Karlsruhe, Germany*

Complete contact information is available at: https://pubs.acs.org/10.1021/acs.est.2c09356

Author Contributions

The manuscript was written through contributions of all authors. All authors have given approval to the final version of the manuscript.

Notes

The authors declare no competing financial interest.

Electronic data created within this study comprises raw data of analytical instruments and raw spectra recorded with an HR-XANES spectrometer. They are stored in the open-access central repository of the KIT (KITopen).

ACKNOWLEDGMENTS

The authors thank Maria do Sameiro Marques Fernandes (Laboratory for Waste Management (LES), Paul Scherrer Institut (PSI)) for the provision of IdP B and helpful comments to the manuscript and Jocelyne Brendle (University Haute-Alsace) for the provision of the IfM. They are grateful for the TEM measurements performed by Oliver Dieste (INE, KIT). They gratefully acknowledge the contribution of Sabrina Gfrerer (Institute for Applied Microbiology, KIT) with fluorescence microscopy. The authors thank Tom Kupcik for the setup of the diffusion experiment. They also thank Martin Glaus (PSI-LES) for the provision of technical drawings and training at the diffusion sample segmentation device. They further thank Jörg Rothe (INE, KIT) and Elke Bohnert (INE, KIT) for technical support. The authors thank the Institute for Beam Physics and Technology (IBPT, KIT) for the operation of the storage ring, the Karlsruhe Research Accelerator (KARA). They acknowledge the KIT Light Source for provision of beamtime. This project has received funding from the European Union's Horizon 2020 research and innovation programme under grant agreement no. 847593. The authors acknowledge funding from the European Research Council (ERC) Consolidator Grant 2020 under the European Union's Horizon 2020 research and innovation programme (grant agreement no. 101003292).

ABBREVIATIONS

CAT-ACT beamline	beamline for catalysis and actinide science
EDX	energy-dispersive X-ray spectroscopy
E_h	redox potential referred to the standard hydrogen electrode
EXAFS	extended X-ray absorption fine structure
HLW	high-level nuclear waste
HR-XANES	high-energy resolution X-ray absorption near-edge structure
IdP	Illite du Puy
ICP−MS	inductively coupled plasma−mass spectrometry
IfM	iron-free synthetic montmorillonite
INE	Institute for Nuclear Waste Disposal
KARA	Karlsruhe research accelerator
KIT	Karlsruhe Institute of Technology
LSC	liquid scintillation counting
SUL-X	Synchrotron Laboratory for Environmental Studies
SWy	Wyoming smectite
TEM	transmission electron microscopy
TOT	tetrahedra octahedra tetrahedra
WL	white line
XAS	X-ray absorption spectroscopy

REFERENCES

(1) Arbeitskreis Auswahlverfahren Endlagerstandorte (AkEnd). Auswahlverfahren für Endlagerstandorte. 2002 https://www.bgr.bund.de/DE/Themen/Endlagerung/Downloads/Standortauswahl/Arbeitskreis_Auswahlverfahren_Endlagerstandorte/kmat_01_akend_data.pdf?__blob=publicationFile&v=5%0A.

(2) Committee on Radioactive Waste Management (CoRWM). Managing our radioactive waste savely; CoRWM Doc 700, 2006 https://www.gov.uk/government/publications/managing-our-radioactive-waste-safely-corwm-doc-700.

(3) *National Cooperative for the Disposal of Radioactive Waste (Nagra)*, Project Opalinus Clay Safety Report, 2002.

(4) Bruno, J.; Ewing, R. C. Spent nuclear fuel. *Elements* **2006**, *2*, 343−349.

(5) Holt, M. Civilian Nuclear Waste Disposal. In *Nuclear Waste: Management, Storage and Disposal*; Nova Science Publishers, Inc., 2020; pp 195−2681.

(6) Kalmykov, S. N.; Kriventsov, V. V.; Teterin, Y. A.; Novikov, A. P. Plutonium and neptunium speciation bound to hydrous ferric oxide colloids. *C. R. Chim.* **2007**, *10*, 1060−1066.

(7) Petrov, V. G.; Fellhauer, D.; Gaona, X.; Dardenne, K.; Rothe, J.; Kalmykov, S. N.; Altmaier, M. Solubility and hydrolysis of Np(V) in dilute to concentrated alkaline NaCl solutions: formation of Na−Np(V)−OH solid phases at 22 °C. *Radiochim. Acta* **2017**, *105*, 1−20.
(8) Jové-Colón, C. F.; Weck, P. F.; Sassani, D. H.; Zheng, L.; Rutqvist, J.; Steefel, C. I.; Kunhiwi, K.; Nakagawa, S.; Houseworht, J.; Birkholzer, J.; Caporuscio, F. A.; Cheshire, M.; Rearick, M. S.; McCarney, M. K.; Zavarin, M.; Benedicto, A.; Kersting, A. B.; Sutton, M.; Jerden, J.; Frey, K. E.; Copple, J. M.; Ebert, W. *Fuel Cycle Research and Development: Evaluation of Used Fuel Disposition in Clay-Bearing Rock (FCRD-UFD--000056)*; Sandia National Laboratories: Albuquerque, New Mexico, 2014.
(9) Neck, V.; Kim, J. I. Solubility and hydrolysis of tetravalent actinides. *Radiochim. Acta* **2001**, *89*, 1−16.
(10) *National Cooperative for the Disposal of Radioactive Waste (Nagra)*; Projekt Opalinuston, Synthese der geowissenschaftlichen Untersuchungsergebnisse; NTB 02-03, 2002.
(11) Zeelmaekers, E.; Honty, M.; Derkowski, A.; Środoń, J.; De Craen, M.; Vandenberghe, N.; Adriaens, R.; Ufer, K.; Wouters, L. Qualitative and quantitative mineralogical composition of the Rupelian Boom Clay in Belgium. *Clay Miner.* **2015**, *50*, 249−272.
(12) Claret, F.; Bauer, A.; Schäfer, T.; Griffault, L.; Lanson, B. Experimental investigation of the interaction of clays with high-pH solutions: A case study from the Callovo-Oxfordian formation, Meuse-Haute Marne underground laboratory (France). *Clays Clay Miner.* **2002**, *50*, 633−646.
(13) Velde, B. *Introduction to Clay Minerals*; Springer Netherlands: Dordrecht, 1992. DOI: 10.1007/978-94-011-2368-6.
(14) Bradbury, M. H.; Baeyens, B. Sorption modelling on illite. Part II: Actinide sorption and linear free energy relationships. *Geochim. Cosmochim. Acta* **2009**, *73*, 1004−1013.
(15) Gorgeon, L. Contribution à la modélisation physico-chimique de la retention de radioeléments à vie longue par des materiaux argileux. Ph.D.Dissertation; Université Paris 6: Paris, 1994.
(16) Marsac, R.; Banik, N. L.; Lützenkirchen, J.; Marquardt, C. M.; Dardenne, K.; Schild, D.; Rothe, J.; Diascorn, A.; Kupcik, T.; Schäfer, T.; Geckeis, H. Neptunium redox speciation at the illite surface. *Geochim. Cosmochim. Acta* **2015**, *152*, 39−51.
(17) Geckeis, H.; Lützenkirchen, J.; Polly, R.; Rabung, T.; Schmidt, M. Mineral−water interface reactions of actinides. *Chem. Rev.* **2013**, *113*, 1016−1062.
(18) Liu, X.; Tournassat, C.; Grangeon, S.; Kalinichev, A. G.; Takahashi, Y.; Marques Fernandes, M. Molecular-level understanding of metal ion retention in clay-rich materials. *Nat. Rev. Earth Environ.* **2022**, *3*, 461−476.
(19) Romanchuk, A. Y.; Kalmykov, S. N.; Novikov, A. P.; Zakharovac, E. V. Regularities of the sorption behavior of actinide ions on mineral colloid particles. *Russ. J. Gen. Chem.* **2011**, *81*, 2029−2038.
(20) Zavarin, M.; Powell, B. A.; Bourbin, M.; Zhao, P.; Kersting, A. B. Np(V) and Pu(V) ion exchange and surface-mediated reduction mechanisms on montmorillonite. *Environ. Sci. Technol.* **2012**, *46*, 2692−2698.
(21) Gautschi, A. Sicherheitsrelevante hydrogeologische Eigenschaften der Tonsteinbarriere eines Schweizer Tiefenlagers für radioaktive Abfälle: Eine Evaluation anhand mehrfacher Argumentationslinien. *Grundwasser* **2017**, *22*, 221−233.
(22) Fröhlich, D. R.; Amayri, S.; Drebert, J.; Reich, T. Influence of humic acid on neptunium(V) sorption and diffusion in Opalinus Clay. *Radiochim. Acta* **2013**, *101*, 553−560.
(23) Reich, T.; Amayri, S.; Börner, P. J. B.; Drebert, J.; Fröhlich, D. R.; Grolimund, D.; Kaplan, U. Speciation of neptunium during sorption and diffusion in natural clay. *J. Phys.: Conf. Ser.* **2016**, *712*, No. 012081.
(24) Wu, T.; Amayri, S.; Drebert, J.; Van Loon, L. R.; Reich, T. Neptunium(V) sorption and diffusion in Opalinus Clay. *Environ. Sci. Technol.* **2009**, *43*, 6567−6571.
(25) Xia, X.; Idemitsu, K.; Arima, T.; Inagaki, Y.; Ishidera, T.; Kurosawa, S.; Iijima, K.; Sato, H. Corrosion of carbon steel in compacted bentonite and its effect on neptunium diffusion under reducing condition. *Appl. Clay Sci.* **2005**, *28*, 89−100.
(26) Rothe, J.; Butorin, S.; Dardenne, K.; Denecke, M. A.; Kienzler, B.; Löble, M.; Metz, V.; Seibert, A.; Steppert, M.; Vitova, T.; Walther, C.; Geckeis, H. The INE-Beamline for actinide science at ANKA. *Rev. Sci. Instrum.* **2012**, *83*, No. 043105.
(27) Pidchenko, I.; Kvashnina, K. O.; Yokosawa, T.; Finck, N.; Bahl, S.; Schild, D.; Polly, R.; Bohnert, E.; Rossberg, A.; Göttlicher, J.; Dardenne, K.; Rothe, J.; Schäfer, T.; Geckeis, H.; Vitova, T. Uranium redox transformations after U(VI) coprecipitation with magnetite nanoparticles. *Environ. Sci. Technol.* **2017**, *51*, 2217−2225.
(28) Vitova, T.; Pidchenko, I.; Fellhauer, D.; Bagus, P. S.; Joly, Y.; Pruessmann, T.; Bahl, S.; Gonzalez-Robles, E.; Rothe, J.; Altmaier, M.; Denecke, M. A.; Geckeis, H. The role of the 5f valence orbitals of early actinides in chemical bonding. *Nat. Commun.* **2017**, *8*, No. 16053.
(29) Vitova, T.; Denecke, M. A.; Göttlicher, J.; Jorissen, K.; Kas, J. J.; Kvashnina, K.; Prüßmann, T.; Rehr, J. J.; Rothe, J. Actinide and lanthanide speciation with high-energy resolution X-ray techniques. *J. Phys.: Conf. Ser.* **2013**, *430*, No. 012117.
(30) Kvashnina, K. O.; Butorin, S. M.; Martin, P.; Glatzel, P. Chemical state of complex uranium oxides. *Phys. Rev. Lett.* **2013**, *111*, No. 253002.
(31) Glatzel, P.; Weng, T.-C. C.; Kvashnina, K.; Swarbrick, J.; Sikora, M.; Gallo, E.; Smolentsev, N.; Mori, R. A. Reflections on hard X-ray photon-in/photon-out spectroscopy for electronic structure studies. *J. Electron Spectros. Relat. Phenom.* **2013**, *188*, 17−25.
(32) Schacherl, B.; Joseph, C.; Lavrova, P.; Beck, A.; Reitz, C.; Pruessmann, T.; Fellhauer, D.; Lee, J.-Y.; Dardenne, K.; Rothe, J.; Geckeis, H.; Vitova, T. Paving the way for examination of coupled redox/solid-liquid interface reactions: 1 ppm Np adsorbed on clay studied by Np M_5-edge HR-XANES spectroscopy. *Anal. Chim. Acta* **2022**, *1202*, No. 339636.
(33) Schacherl, B.; Prüssmann, T.; Dardenne, K.; Hardock, K.; Krepper, V.; Rothe, J.; Vitova, T.; Geckeis, H. Implementation of cryogenic tender X-ray HR-XANES spectroscopy at the ACT station of the CAT-ACT beamline at the KIT Light Source. *J. Synchrotron Radiat.* **2022**, *29*, 80−88.
(34) Vitova, T.; Pidchenko, I.; Schild, D.; Prüßmann, T.; Montoya, V.; Fellhauer, D.; Gaona, X.; Bohnert, E.; Rothe, J.; Baker, R. J.; Geckeis, H. Competitive reaction of neptunium(V) and uranium(VI) in potassium−sodium carbonate-rich aqueous media: Speciation study with a focus on high-resolution X-ray spectroscopy. *Inorg. Chem.* **2020**, *59*, 8−22.
(35) Bertrand, P. A.; Choppin, G. R. Separation of actinides in different oxidation states by solvent extraction. *Radiochim. Acta* **1982**, *31*, 135−137.
(36) Glaus, M. A.; Aertsens, M.; Appelo, C. A. J.; Kupcik, T.; Maes, N.; Van Laer, L.; Van Loon, L. R. Cation diffusion in the electrical double layer enhances the mass transfer rates for Sr^{2+}, Co^{2+} and Zn^{2+} in compacted illite. *Geochim. Cosmochim. Acta* **2015**, *165*, 376−388.
(37) Montoya, V.; Baeyens, B.; Glaus, M. A.; Kupcik, T.; Fernandes, M. M.; Van Laer, L.; Bruggeman, C.; Maes, N.; Schäfer, T. Sorption of Sr, Co and Zn on illite: Batch experiments and modelling including Co in-diffusion measurements on compacted samples. *Geochim. Cosmochim. Acta* **2018**, *223*, 1−20.
(38) Gabis, V. Etude mineralogique et geochimique de la serie sedimentaire oligocene du Velay. *Bull. Minéral.* **1963**, *86*, 315−354.
(39) Bradbury, M. H.; Baeyens, B. Sorption modelling on illite Part I: Titration measurements and the sorption of Ni, Co, Eu and Sn. *Geochim. Cosmochim. Acta* **2009**, *73*, 990−1003.
(40) Reinholdt, M.; Miehé-Brendlé, J.; Delmotte, L.; Tuilier, M.-H.; le Dred, R.; Cortès, R.; Flank, A.-M. Fluorine route synthesis of montmorillonites containing Mg or Zn and characterization by XRD, thermal analysis, MAS NMR, and EXAFS spectroscopy. *Eur. J. Inorg. Chem.* **2001**, *2001*, 2831−2841.
(41) Reinholdt, M.; Miehé-Brendlé, J.; Delmotte, L.; Le Dred, R.; Tuilier, M.-H. Synthesis and characterization of montmorillonite-type phyllosilicates in a fluoride medium. *Clay Miner.* **2005**, *40*, 177−190.

(42) Fellhauer, D.; Rothe, J.; Altmaier, M.; Neck, V.; Runke, J.; Wiss, T.; Fanghänel, T. Np(V) solubility, speciation and solid phase formation in alkaline $CaCl_2$ solutions. Part I: Experimental results. *Radiochim. Acta* **2016**, *104*, 355−379.
(43) Parkhurst, D. L.; Appelo, C. A. J. *Description of Input and Examples for PHREEQC Version 3--A Computer Program for Speciation, Batch- Reaction, One-Dimensional Transport, and Inverse Geochemical Calculations: U.S. Geological Survey Techniques and Methods*, Water-Resources Investigations Report; U.S. Geological Survey: Denver, CO, 2013; p 497.
(44) Van Loon, L. R.; Soler, J. M.; Bradbury, M. H. Diffusion of HTO, $^{36}Cl^-$ and $^{125}I^-$ in Opalinus Clay samples from Mont Terri: Effect of confining pressure. *J. Contam. Hydrol.* **2003**, *61*, 73−83.
(45) Beck, A.; Bohnert, E.; Fellhauer, D.; Hardock, K.; Joseph, C.; Krepper, V.; Marquardt, C.; Rieder, F.; Rothe, J.; Schacherl, B.; Vitova, T. Diffusion. In *Annual Report 2018/19 Institute for Nuclear Waste Disposal*; Geckeis, H.; Altmaier, M.; Fanghänel, S., Eds.; KIT Scientific Publishing: Karlsruhe, 2020; Chapter 5.2, pp 33−35.
(46) Zimina, A.; Dardenne, K.; Denecke, M. A.; Doronkin, D. E.; Huttel, E.; Lichtenberg, H.; Mangold, S.; Prüßmann, T.; Rothe, J.; Spangenberg, T.; Steininger, R.; Vitova, T.; Geckeis, H.; Grunwaldt, J.-D. CAT-ACT — A new highly versatile X-ray spectroscopy beamline for catalysis and radionuclide science at the KIT synchrotron light facility ANKA. *Rev. Sci. Instrum.* **2017**, *88*, No. 113113.
(47) Aran, E. KIT, IPS - SUL-X. https://www.ips.kit.edu/5931.php. (accessed Jul 28, 2018).
(48) Ravel, B.; Newville, M. ATHENA, ARTEMIS, HEPHAESTUS: Data analysis for X-ray absorption spectroscopy using IFEFFIT. *J. Synchrotron Radiat.* **2005**, *12*, 537−541.
(49) Gorski, C. A.; Aeschbacher, M.; Soltermann, D.; Voegelin, A.; Baeyens, B.; Fernandes, M. M.; Hofstetter, T. B.; Sander, M. Redox properties of structural Fe in clay minerals. 1. electrochemical quantification of electron-donating and -accepting capacities of smectites. *Environ. Sci. Technol.* **2012**, *46*, 9360−9368.
(50) Huang, J.; Jones, A.; Waite, T. D.; Chen, Y.; Huang, X.; Rosso, K. M.; Kappler, A.; Mansor, M.; Tratnyek, P. G.; Zhang, H. Fe(II) redox chemistry in the environment. *Chem. Rev.* **2021**, *121*, 8161−8233.
(51) Asaad, A.; Hubert, F.; Dazas, B.; Razafitianamaharavo, A.; Brunet, J.; Glaus, M. A.; Savoye, S.; Ferrage, E.; Tertre, E. A baseline study of mineralogical and morphological properties of different size fractions of illite du Puy. *Appl. Clay Sci.* **2022**, *224*, No. 106517.
(52) Physical and Chemical Data of Source Clays − The Clay Minerals Society. https://www.clays.org/sourceclays_data/. (accessed May 30, 2022).
(53) Schnurr, A. Untersuchungen zur Radionuklidsorption an Tonmineraloberflächen bei hohen Ionenstärken. Ph.D. Dissertation; Karlsruhe Institute of Technology (KIT): Karlsruhe, 2015.
(54) Soltermann, D.; Fernandes, M. M.; Baeyens, B.; Dähn, R.; Miehé-Brendlé, J.; Wehrli, B.; Bradbury, M. H. Fe(II) sorption on a synthetic montmorillonite. A combined macroscopic and spectroscopic study. *Environ. Sci. Technol.* **2013**, *47*, 6978−6986.
(55) Bradbury, M. H.; Baeyens, B. A mechanistic description of Ni and Zn sorption on Na-montmorillonite Part II: Modelling. *J. Contam. Hydrol.* **1997**, *27*, 223−248.
(56) Payne, T. E.; Brendler, V.; Comarmond, M. J.; Nebelung, C. Assessment of surface area normalisation for interpreting distribution coefficients (K_d) for uranium sorption. *J. Environ. Radioact.* **2011**, *102*, 888−895.
(57) Bradbury, M. H.; Baeyens, B. Modelling sorption data for the actinides Am(III), Np(V) and Pa(V) on montmorillonite. *Radiochim. Acta* **2006**, *94*, 619−625.
(58) Bradbury, M. H.; Baeyens, B. *Experimental and Modelling Investigations on Na-illite: Acid-Base Behaviour and the Sorption of Strontium, Nickel, Europium and Uranyl; PSI 05-02*; Paul Scherrer Institute (PSI), 2005.
(59) Vitova, T.; Faizova, R.; Amaro-Estrada, J. I.; Maron, L.; Pruessmann, T.; Neill, T.; Beck, A.; Schacherl, B.; Tirani, F. F.; Mazzanti, M. The mechanism of Fe induced bond stability of uranyl(V). *Chem. Sci.* **2022**, *13*, 11038−11047.
(60) Ma, B.; Charlet, L.; Fernandez-Martinez, A.; Kang, M.; Madé, B. A review of the retention mechanisms of redox-sensitive radionuclides in multi-barrier systems. *Appl. Geochem.* **2019**, *100*, 414−431.
(61) Kumar, S.; Rothe, J.; Finck, N.; Vitova, T.; Dardenne, K.; Beck, A.; Schild, D.; Geckeis, H. Effect of manganese on the speciation of neptunium(V) on manganese doped magnetites. *Colloids Surf., A* **2022**, *635*, No. 128105.
(62) Antonio, M. R.; Soderholm, L.; Williams, C. W.; Blaudeau, J.-P. P.; Bursten, B. E. Neptunium redox speciation. *Radiochim. Acta* **2001**, *89*, 17−25.
(63) Ikeda-Ohno, A.; Hennig, C.; Rossberg, A. A.; Funke, H.; Scheinost, A. C.; Bernhard, G.; Yaita, T. Electrochemical and complexation behavior of neptunium in aqueous perchlorate and nitrate solutions. *Inorg. Chem.* **2008**, *47*, 8294−8305.
(64) Gückel, K.; Rossberg, A.; Müller, K.; Brendler, V.; Bernhard, G.; Foerstendorf, H. Spectroscopic identification of binary and ternary surface complexes of Np(V) on gibbsite. *Environ. Sci. Technol.* **2013**, *47*, 14418−14425.
(65) Elo, O.; Müller, K.; Ikeda-Ohno, A.; Bok, F.; Scheinost, A. C.; Hölttä, P.; Huittinen, N. Batch sorption and spectroscopic speciation studies of neptunium uptake by montmorillonite and corundum. *Geochim. Cosmochim. Acta* **2017**, *198*, 168−181.
(66) Arai, Y.; Moran, P. B.; Honeyman, B. D.; Davis, J. A. In situ spectroscopic evidence for neptunium(V)-carbonate inner-sphere and outer-sphere ternary surface complexes on hematite surfaces. *Environ. Sci. Technol.* **2007**, *41*, 3940−3944.
(67) Virtanen, S.; Bok, F.; Ikeda-Ohno, A.; Rossberg, A.; Lützenkirchen, J.; Rabung, T.; Lehto, J.; Huittinen, N. The specific sorption of Np(V) on the corundum (α-Al_2O_3) surface in the presence of trivalent lanthanides Eu(III) and Gd(III): A batch sorption and XAS study. *J. Colloid Interface Sci.* **2016**, *483*, 334−342.
(68) Denecke, M. A.; Marquardt, C. M.; Rothe, J.; Dardenne, K.; Jensen, M. P. XAFS study of actinide coordination structure in Np(IV)-fulvates. *J. Nucl. Sci. Technol.* **2002**, *39*, 410−413.
(69) Rabung, T.; Pierret, M. C.; Bauer, A.; Geckeis, H.; Bradbury, M. H.; Baeyens, B. Sorption of Eu(III)/Cm(III) on Ca-montmorillonite and Na-illite. Part 1: Batch sorption and time-resolved laser fluorescence spectroscopy experiments. *Geochim. Cosmochim. Acta* **2005**, *69*, 5393−5402.
(70) Latta, D. E.; Neumann, A.; Premaratne, W. A. P. J.; Scherer, M. M. Fe(II)-Fe(III) electron transfer in a clay mineral with low Fe content. *ACS Earth Space Chem.* **2017**, *1*, 197−208.

https://doi.org/10.1021/acs.est.2c09356
Environ. Sci. Technol. 2023, 57, 11185−11194